

Photoinduced phases in jacutingaite monolayer

Mohammad Alipourzadeh 


Department of Physics, Faculty of Science, Shahid Chamran University of Ahvaz, 6135743135 Ahvaz, Iran

Yaser Hajati *

*Institut für Physik, Martin-Luther Universität Halle-Wittenberg, D-06099 Halle, Germany
and Department of Physics, Faculty of Science, Shahid Chamran University of Ahvaz, 6135743135 Ahvaz, Iran*

Jamal Berakdar 

Institut für Physik, Martin-Luther Universität Halle-Wittenberg, D-06099 Halle, Germany

 (Received 26 July 2023; revised 7 October 2023; accepted 17 November 2023; published 19 December 2023)

The topological phases of monolayer jacutingaite (Pt_2HgSe_3) under off-resonance high-frequency and high-intensity laser irradiation and staggered sublattice potential V are investigated. The various steady-state phases are realized by an appropriate choice of the off-resonance circularly polarized laser field parameters and the staggered sublattice potential. By tuning the band gap through V and/or laser intensity, a phase diagram is deduced and explained. Increasing the laser intensity at $V = 0$ leads to a photoinduced quantum Hall insulator state with chiral edge currents, while increasing V in the absence of laser field changes the phase from quantum spin Hall to quantum valley Hall phases. An electromagnetically induced, steady-state spin-polarized quantum Hall state is predicted at particular values of V and the laser intensity relative to the spin-orbit coupling strength. The emergence of the topological phases is corroborated by calculating the Chern numbers of each band, and the Hall conductivity at zero temperature. Calculations of the Nernst coefficient give further evidence at nonzero temperatures. Along the phase boundaries, we observe steady-state single Dirac cone, spin-polarized, and spin-valley-polarized metal states which may be exploited in use of jacutingaites in spin and valleytronics.

DOI: [10.1103/PhysRevResearch.5.043263](https://doi.org/10.1103/PhysRevResearch.5.043263)

I. INTRODUCTION

Much research has been devoted in recent years to topological materials that exhibit for instance quantum spin Hall (QSH) states with prospective use in low-power energy consumption devices and quantum computing [1]. QSH insulators support edge states which are theoretically immune to backscattering. To establish a QSH system, certain key characteristics are required. First, a hexagonal lattice structure helps facilitating a sizable spin-orbit coupling (SOC) [2]. The Kane-Mele insulator (KMI) is an example of such a system. Secondly, for applications, the material should have a topological gap that persists to room temperature to ensure stability at ambient conditions [1]. Additionally, weak intralayer interactions, specifically of the van der Waals type, are desirable for enabling exfoliation of thin layers from bulk materials [3].

Graphene and silicene have been considered as potential candidates of KMIs [2,4–7]. Their SOC strength is however rather weak. Monolayers of transition metal dichalcogenides (TMDCs) in the $1T'$ phase also exhibit significant SOC

which is beneficial for achieving a QSH state [8,9]. However, TMDCs are challenging candidates from an application point of view due to their metastable nature [9] and susceptibility to oxidation which limits their use.

Jacutingaite [10], a mineral characterized by the general formula Pt_2AX_3 ($A = \text{Hg, Cd}$ and $X = \text{S, Se}$) is exfoliable and consists of a Pt layer sandwiched between two layers of Se and Hg ordering in a honeycomb structure [11], similar to silicene and graphene [12,13]. Monolayer jacutingaite serves as a KMI realization at room temperature with a relatively large SOC-induced gap of around 160 meV [14–16]. Additionally, it is highly stable, making it a potentially good candidate for various applications.

Various external probes can be used to adjust the band gap in two-dimensional (2D) materials such as electric [17–19] or antiferromagnetic exchange fields [20]. Also, off-resonance circularly polarized laser fields can be used to tune the steady-state properties. Experimental [21–23] and theoretical [24–30] studies on TMDCs confirmed that off-resonance light can manipulate spin and valley degrees of freedom. A key feature is that, in off-resonance and high-frequency approximation, the intensity and photonic spin angular momentum can modify the charge and spin degrees of freedom (in presence of SOC). Time reversal symmetry ensures that left (right) circular polarization interacts with the K (K') valley.

Ezawa [4] has studied the phases of an irradiated silicene sheet in the presence of an electric field and uncovered various distinct phases depending on the fields' parameters. The

*yaserhajati@gmail.com

Published by the American Physical Society under the terms of the Creative Commons Attribution 4.0 International license. Further distribution of this work must maintain attribution to the author(s) and the published article's title, journal citation, and DOI.

heterostructure $\text{Pt}_2\text{AX}_3/\text{CrI}_3$ is a valley-polarized Chern insulator with a large orbital magnetization that may induce a measurable optical Kerr effect [12]. Recently, the topological phase shifting of monolayer jacutingaite under magnetic exchange interactions and staggered sublattice potential is investigated [13]. It is found that in the presence of the Rashba interaction in certain parameter regimes, the system exhibits both quantum anomalous Hall and quantum valley Hall effects, simultaneously. A similar study on the familiar topological insulator Bi_2Se_3 shows that when thin films are irradiated with off-resonance light, distinct phases emerge in the phase diagram depending on frequency, intensity, and polarization of the off-resonance light [31]. A recent study on the jacutingaite family also shows that induced spin splittings, Berry curvature (BC), and spin texture between two valleys can be swapped upon reversing the electric field from positive to negative without destroying Z_2 topological hallmarks [32]. However, the impact of off-resonance light on the phase transition of nonmagnetic jacutingaites has not been extensively discussed so far.

In this paper, we investigate the phases in a monolayer of jacutingaite. We utilized the Kane-Mele model and consider the effects of a sublattice staggered potential (V) that arises when applying a vertical electric field (E_z) and off-resonance light imparting effectively an energy Δ_Ω to the system. By analyzing the total (C), spin (C_s), and valley Chern numbers (C_v), we demonstrate that jacutingaites exhibit a wide range of topological phases. Our findings reveal that by appropriately modulating the fields, the system can undergo transitions between the QSH, the quantum valley Hall (QVH), the photoinduced quantum Hall insulator (P-QHI), and the electromagnetic-induced spin-polarized quantum Hall insulator (S-QHI) phases. Moreover, we identify the emergence of electromagnetically adjustable single Dirac cone (SDC), spin-polarized metal (SPM), and spin-valley-polarized metal (SVPM) states at the phase boundaries. Furthermore, we calculate the spin/valley anomalous Nernst coefficient (ANC) for further insight and validation at elevated temperatures.

II. FORMALISM

We consider a transverse circularly polarized laser field impinging perpendicular onto the 2D material. Within the dipole approximation the field's vector potential reads $\mathbf{A}(t) = A(\sin(\pm\omega t), \cos(\pm\omega t))$, where $\omega = 2\pi/T$ is the frequency of light and the \pm sign corresponds to the right and left circular polarization, respectively. $|A| = |E_0/\omega|$ with E_0 being the amplitude of the laser's electric field and the pulse duration is assumed much larger than the period T . In the high-intensity, high-frequency regime, based on Floquet analysis [33] it follows that a steady-state electronic structure is established in the presence of the laser [4,34]. More precisely for $eAv_f/\hbar\omega \ll 1$ (where $v_f = 3 \times 10^5$ m/s is the Fermi velocity in monolayer jacutingaite) and after averaging over the high-frequency dynamics, the steady-state dynamic of the monolayer jacutingaite in the presence of off-resonance light and perpendicular electric field is captured by the effective Hamiltonian [4,13,35]

$$H_{\eta,s_z} = \hbar v_f(\eta k_x \sigma_x + k_y \sigma_y) + \eta s_z \lambda \sigma_z + \eta \Delta_\Omega \sigma_z + V \sigma_z, \quad (1)$$

where k_x and k_y are the components of the wave vector k with $k = \sqrt{k_x^2 + k_y^2}$, and $\Delta_\Omega = (ev_f A)^2/\hbar\omega$ is the energy contribution due to the interaction with the laser field. Here, $s_z = +1$ (-1) refers to the electron spin up (down), $\eta = +1$ (-1) corresponds to the K (K') valley, and $\sigma_{x,y,z}$ is the Pauli matrix in the sublattice space. In Eq. (1), the first term resembles a massless graphene-type Hamiltonian [36], and the second one is the Kane-Mele SOC with $\lambda = 81.2$ meV [14], which is almost 20 times larger than that in silicene [37], and respects both time reversal and inversion symmetries. Jacutingaite monolayer exhibits different structural parameters and Fermi velocity than silicene or graphene (such as the lattice constant) which have consequences for the topological and transport properties. First-principles studies on the band gap and its tunability do exist (e.g., Refs. [14,38]). Here, the large separation between the high-symmetry lines in the momentum space and the relatively small difference between the conduction band minimum point of K and M points indicate that our remain conclusions are valid at low temperatures.

The eigenvalues of Eq. (1) can be written as

$$E_{\eta,s_z}^n = n\sqrt{(\hbar v_f k)^2 + (\Delta_{\eta,s_z})^2}. \quad (2)$$

The mass term $\Delta_{\eta,s_z} = \eta \Delta_\Omega + \eta s_z \lambda + V$ indicates the effective gap, and $n = \pm$ stands for the conduction and valence bands, respectively.

The velocity operator $\mathbf{v} = \partial H_{\eta,s_z}/\partial \mathbf{p}$ [13] has two components: $v_x = \eta v_f \sigma_x$ and $v_y = v_f \sigma_y$. Having the velocity operators and the eigenvalues, the BC is obtained as [13,39,40]

$$\Omega_{\eta,s_z}^n(k) = -2\hbar^2 \text{Im} \sum_{n \neq n'} f_{nk} \frac{\langle u_{nk} | v_x | u_{n'k} \rangle \langle u_{n'k} | v_y | u_{nk} \rangle}{(E_{\eta,s_z}^n - E_{\eta,s_z}^{n'})^2}, \quad (3)$$

in which $f_{nk} = [1 + \exp(E_{\eta,s_z}^n - E_f)/k_B T]^{-1}$ is the Fermi-Dirac distribution function for the n th band with Fermi energy of E_f , and u_{nk} is the eigenstate of Eq. (1). Here, we used the condition $v_{x(y),n;n'}(k) = v_{x(y),n;n'}^*(k)$, due to the Hermiticity of $v_{x,y}$.

Generally, the spin-valley-resolved Hall conductivity at zero temperature can be obtained as

$$\sigma_{\eta,s_z} = \frac{e^2}{h} \int d^2k \Omega_{\eta,s_z}^n. \quad (4)$$

In the insulating regime when the Fermi level lies in the bulk gap, the spin-valley-resolved Hall conductivity is given as $\sigma_{\eta,s_z} = e^2/h C_{\eta,s_z}$, in which C_{η,s_z} is the spin-valley-resolved Chern number and defined as

$$C_{\eta,s_z} = \frac{1}{2\pi} \int d^2k \Omega_{\eta,s_z}^n. \quad (5)$$

In the band gap, for monolayer jacutingaite the aforementioned definition could be simplified to

$$C_{\eta,s_z} = \frac{\eta}{2} \text{sgn}(\Delta_{\eta,s_z}), \quad (6)$$

where $\text{sgn}(x)$ is the sign function. The charge Chern number and spin Chern number are both topological invariants utilized for indexing a topological insulator phase [4,41]. The spin and valley Chern numbers are given by $C_s = (C_\uparrow - C_\downarrow)/2$ and $C_v = (C_K - C_{K'})/2$, respectively, in which $C_{\uparrow(\downarrow)} = \sum_{\eta} C_{\eta,\uparrow(\downarrow)}$ and $C_{K(K')} = \sum_{s_z} C_{K,s_z(K',s_z)}$. Similarly,

we define $\sigma_{\uparrow(\downarrow)} = \sum_{\eta} \sigma_{\eta, \uparrow(\downarrow)}$ and $\sigma_{K(K')} = \sum_{s_z} \sigma_{K, s_z(K', s_z)}$. Accordingly, the total Chern number (C) is the sum of all spin-valley-resolved Chern numbers: $C = \sum_{\eta, s_z} C_{\eta, s_z}$.

Note that if the Fermi energy falls within a band, the Chern number is not defined. Regardless, Eq. (4) can still provide the Hall conductivity.

From the velocity and the entropy density follows the spin-valley resolved ANC as [42,43]

$$\alpha_{\eta, s_z}^n = \frac{ek_B}{2\pi\hbar} \sum_n \int \Omega_{\eta, s_z}^n(k) S_{\eta, s_z}^n(k) dk^2, \quad (7)$$

in which $S_{\eta, s_z}^n(k)$ is the entropy density given by $S_{\eta, s_z}^n(k) = -f_n(k) \ln f_n(k) - [1 - f_n(k)] \ln[1 - f_n(k)]$. The total ANC (TANC) can be calculated by summing over all spin-valley resolved ANCs and the spin ANC (SANC) or valley ANC (VANC) are defined as $\alpha_s = \alpha_{\uparrow} - \alpha_{\downarrow}$ and $\alpha_v = \alpha_K - \alpha_{K'}$, respectively.

It should be noted that the phase terminology used here (in line with the literature) is meant to simplify the classifications of the results. We are not dealing with ground-state quantum or thermal phase transitions but with nonequilibrium phenomena that occur in the presence of the laser. In addition, we rely on the validity of an effective single-particle description of the system that yields band structure from which we infer the transport coefficients under the assumptions that the external perturbations are weak. Generally, stronger perturbations may invalidate the single-particle picture (even for weakly interacting systems in the ground state) as well as the linear response approach to transport. When an effective single-particle approach breaks down, we cannot rely on the above approach for the equilibrium of the system. For dealing with many-body effects under the influence of strong external perturbations and beyond the linear response (which is out of the scope of this paper) one has to resort to other methods such as nonequilibrium Green's functions.

III. RESULTS AND DISCUSSION

In Fig. 1, the numerical results for the phase transitions in monolayer jacutingaite show how varying V and Δ_{Ω} impact the system's topological phase. The combined index (C , C_s , C_v) labels the different regions or phases indicated also by the different colors. Additionally, for the arbitrary marked points P1–P4 (C1–C4) we calculated the energy spectrum and other topological properties and we display them in the subsequent figures. Given that both V and Δ_{Ω} affect the effective gap, the phase changes occur along both directions, and there are significant differences in Chern numbers arising from their varying roles in the Hamiltonian. In the case of unperturbed jacutingaite (i.e., when $V = \Delta_{\Omega} = 0$), which is labeled by the P1 point in Fig. 1, it is seen that $C_{\uparrow} = 1$ and $C_{\downarrow} = -1$, resulting in $C_s = 1$, while $C = C_v = 0$, leading to a QSH phase that originates from the SOC-induced band gap of the material. This is in agreement with what has been reported in Ref. [13]. However, neglecting the SOC closes the band gap, leading to a semimetallic behavior, as pointed out in Ref. [32].

Increasing V or Δ_{Ω} to values under λ does not change the phase since under this condition, the gap remains open and supports the QSH phase. However, at $\Delta_{\Omega} = 0$, when $V = \lambda$ is applied, the effective gap $|V + \eta s_z \lambda|$ becomes zero for

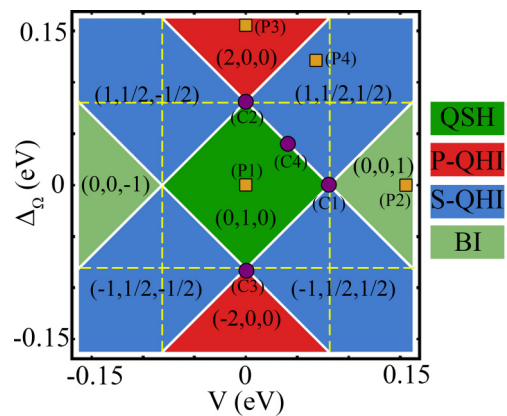


FIG. 1. The phase diagram as a function of the parameters (V , Δ_{Ω}). The white lines indicate the phase boundaries and the yellow ones refer to $\Delta_{\Omega}(V) = \lambda = 0.0821$ eV. Different colors label different phases as stated to the right of the graph. The numbers in each region stand for the combined index (C , C_s , C_v). P1–P4 and C1–C4 are arbitrary chosen points at which the system will be studied in depth in subsequent figures.

$\eta \neq s_z$, leading to a gap closure (see the C1 point in Fig. 1). Increasing V further, the phase changes from QSH to a band insulator (BI). When the gap closes and reopens by electric field tuning, the spin Chern number vanishes while the valley one becomes 1, indicating the BI phase is related to the QVH state (for instance, see the P2 point in Fig. 1).

Conversely, applying $\Delta_{\Omega} > \lambda$ by itself does not change the valley Chern number due to the valley index in the Chern number's definition [see Eq. (6)]. Instead, it substitutes $C = 0$ with $C = 2$ via $C_{\uparrow} = C_{\downarrow} = C_K = C_{K'} = 1$, resulting in a quantum anomalous Hall effect caused by light, namely a P-QHI, as observed in the P3 point of Fig. 1. When both fields are switched on and are strong enough, i.e., $|\pm V \pm \Delta_{\Omega}| > \lambda$, the spin- and valley-resolved Chern numbers become $C_{\uparrow} = 1$, $C_{\downarrow} = 0$, $C_K = 1$, and $C_{K'} = 0$ leading to the emergence of an electromagnetically induced S-QHI. Interestingly, reversing the sign of V (Δ_{Ω}) changes the sign of C_v (C), which can be attributed to the role of this field in the Hamiltonian.

As seen in Eq. (1), the electric field does not couple with spin or valley indices and only relies on the band type (valence or conduction). However, in addition to band coupling, off-resonance light couples effectively to the valley index. At first glance, the phase diagram illustrated in Fig. 1 may bear resemblance to that of silicene [4] or germanene [35]. Nevertheless, owing to the relatively robust strength of SOC in monolayer jacutingaite, there exists a considerably broader spectrum of (V , Δ_{Ω}) ranges within which each phase manifests itself.

To demonstrate how various fields impact the system's effective gap, we present a detailed band structure around K and K' valleys at different parameter regimes in Fig. 2 using the model demonstrated in Eq. (2). In the absence of both fields (i.e., point P1 in the phase diagram), the bands display spin and valley degeneracy with the same gap of 2λ in both valleys due to SOC [see Fig. 2(e)]. This result is consistent with what has been reported in Refs. [13,32], thus validating our model. By adjusting V and Δ_{Ω} , which contribute to the effective gap, the band gap can be tuned, similar to what has been observed

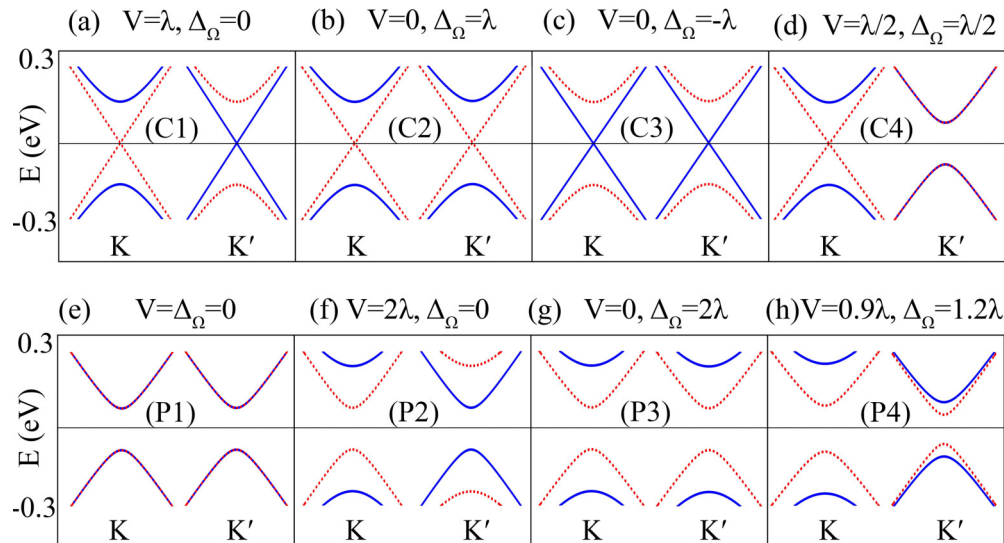


FIG. 2. Band structure of jacutingaites at the K and K' valleys for different parameter regimes as labeled on top of each panel. The corresponding point in the phase diagram is indicated in Fig. 1. The blue and red lines refer to spin up and down energy bands, respectively. The black horizontal line denotes the Fermi energy $E_f = 0$.

in silicene [44,45]. Applying $V < \lambda$ does not close the gap, but when $V = \lambda$ is applied, the gap closes for a specific spin state at each valley, resulting in a SVPM state, as depicted in Fig. 2(a), and coincides with the C1 point in the phase diagram. This indicates that the structure behaves metallic at $V = \lambda$, but the band structure is not the same for both valleys. It should be noted that switching $V \rightarrow -V$ reverses the band structure (not shown here). Conversely, applying $\Delta_\Omega = \pm\lambda$ (corresponding to C2 and C3 points in the phase diagram) closes the band gap for a certain spin state in both valleys, leading to a SPM state, as shown in Figs. 2(b) and 2(c). This may be useful for applications in spintronics in that it can provide a laser-controllable spin-polarized current across a wide energy range.

The difference between the effects of V and Δ_Ω can be explained by the Hamiltonian given in Eq. (1). Although both of these parameters contribute to the effective gap (Δ_{η,s_z}), the laser interacts with the valley index while the electric field is a spin-valley-independent parameter. Thus, when the system is only laser irradiated, the effective gap term becomes $(\eta s_z \lambda + \eta \Delta_\Omega)^2$. Therefore, at $\Delta_\Omega = \pm\lambda$, the effective gap becomes the same for both valleys. On the other hand, at $\Delta_\Omega = 0$ and $V = \pm\lambda$, the value of the effective gap is distinguishable for two valleys. Interestingly, as shown in Figs. 2(b) and 2(c), the polarity of the light can reverse the spin state of the closed gap. When both fields are turned on and set at $\lambda/2$ (coinciding with the C4 point), the gap of a particular valley closes while that of the opposite valley remains open, indicating a SDC state, as seen in Fig. 2(d). The SDC state can appear in different types depending on the chosen parameters [4]. However, it is generally observed when $|\pm V \pm \Delta_\Omega| = \lambda$ is satisfied. The phase remains unchanged when $V < \lambda$ and $\Delta_\Omega < \lambda$ are applied. However, increasing V (Δ_Ω) beyond λ reopens the gap, and the system enters the QVH (P-QHI) phase, as seen in Fig. 2(f) [Fig. 2(g)]. The emergence of these phases is verified in the remaining figures by calculating the Chern number and

Hall conductivity. Finally, when the sum of both fields exceeds the SOC value, i.e., $|\pm V \pm \Delta_\Omega| > \lambda$, all degeneracies are broken, leading to a S-QHI phase, as illustrated in Fig. 2(h) and marked by the P4 point in Fig. 1. The system at this condition can act as an effective spin-valley filter. In fact, by appropriately setting the Fermi energy, only one spin-valley energy band can be made to touch the Fermi level.

For an overview, the predicted phases as indicated by spin- and valley-resolved Chern numbers ($C_\uparrow, C_\downarrow, C_K, C_{K'}$) are presented in Table I. For $|\pm V \pm \Delta_\Omega| < \lambda$, the system displays a QSH phase (for instance, see the P1 point in Fig. 1), where the edge states of spin up and spin down exhibit opposing current directions, namely helical modes. In this case, the valley Chern numbers are equal to zero, which is consistent with previous studies on this material [13,32] as well as its counterpart, silicene [35]. On the other hand, when $\Delta_\Omega > \lambda$ ($V > \lambda$) is applied, the spin up and spin down Chern number becomes 1 (0). Also, at $\Delta_\Omega > \lambda$ the K and K' valley Chern numbers equally become 1, while at $V > \lambda$ they show 1 and -1 for K and K' valleys, respectively, indicating a P-QHI phase for the former and QVH for the latter. It should be noted that since the valley Chern number does not vanish at the BI phase, it can be considered as a type of QVH phase. When $|\pm V \pm \Delta_\Omega| > \lambda$, the system enters a S-QHI phase with a zero Chern number in one valley and one spin, indicating that the current originates solely from one spin and valley edge mode.

To confirm the obtained Chern numbers, we have calculated the spin and valley Hall conductivities at zero temperature using the Kubo formula [13]. As shown in Eq. (5), the spin-valley resolved Hall conductivity is proportional to the Chern numbers when the Fermi energy lies within the gap. Figure 3 displays the spin and valley Hall conductivities as a function of Fermi energy at zero temperatures ($T = 0$). The Hall conductivities drop to zero when the Fermi level is far from the gap, which can be attributed to the

TABLE I. Spin- and valley-resolved and spin (valley) Chern numbers for different parameter regimes of the proposed structure at $E_f = 0$.

C_\uparrow	C_\downarrow	C_s	C_K	$C_{K'}$	C_v	Phase	Spin modes	Parameter regime
1	-1	1	0	0	0	QSH	Both spins have helical edge modes	$V < \lambda, \Delta_\Omega = 0$
0	0	0	1	-1	1	BI (QVH)	No spin edge modes	$V > \lambda, \Delta_\Omega = 0$
1	-1	1	0	0	0	QSH	Both spins have helical edge modes	$V = 0, \Delta_\Omega < \lambda$
1	1	0	1	1	0	P-QHI	Both spins have chiral edge modes	$V = 0, \Delta_\Omega > \lambda$
1	-1	1	0	0	0	QSH	Both spins have helical edge modes	$V + \Delta_\Omega < \lambda$
1	0	1	1	0	1	S-QHI	Only one spin state has edge modes	$V + \Delta_\Omega > \lambda$

scattering process. Since we are interested in the topological phases, we focus mainly on the gap region and set $E_f = 0$ while selecting the parameters that keep the gap open for at least one spin-valley state. At $V = \Delta_\Omega = 0$, corresponding to the P1 point in the phase diagram (Fig. 1), the Hall conductivity is zero for both valleys and ± 1 for $s_z = \pm 1$ spin states, confirming the helical currents predicted in Table I and thereby verifying the QSH phase shown in Fig. 1. It should be noted that the region where $\sigma_s = \pm 1$ coincides with the gap region presented in Fig. 2(e). The spin degeneracy leads to equal energy ranges in which $\sigma_s = \pm 1$ for both spin states and causes symmetry between the two spin Hall conductivity curves, as demonstrated in Figs. 3(a) and 3(b).

As predicted in the phase diagram at the P2 point and shown in Fig. 3(c), application of $V > \lambda$ destroys the spin Hall conductivity in the gap. When $V > \lambda$, the effective gap is always positive, leading to the sign function in the Chern number's definition being 1 for all spin-valley flavors [see Eq. (6)]. However, the valley index coupled to the sign function results in different sign of the Chern numbers (with same values) for different valleys, causing the summation of spin Chern

numbers to become zero. On the other hand, the valley Chern numbers maximize for the same reason. This observation can also be justified by the sign of BC. The BC has opposite signs for a specific spin state at different valleys, resulting in their integration canceling each other and destroying the spin Hall conductivities.

Conversely, application of off-resonance light when $\Delta_\Omega > \lambda$ maximizes the Hall conductivities for all spin and valley states due to the same reasons described above. Since the light is coupled to the valley index, it can produce chiral edge currents, as shown in Figs. 3(e) and 3(f), thereby verifying the emergence of the P-QHI phase at the P3 point. Interestingly, application of the laser only does not break the valley Hall degeneracy. By applying $|V + \Delta_\Omega| > \lambda$ the conductivity of spin up and K valley maximizes while that of the spin down and K' valley vanishes within the gap, indicating the emergence of the S-QHI phase, as depicted at the P4 point of the phase diagram [see Figs. 1, 2(g), and 2(h)].

Figure 4 shows the Hall conductivities dependence at the gap for $E_f = 0$ with respect to V or Δ_Ω . Figures 1 and 3 evidence that when $\Delta_\Omega = 0$ the phase cannot be shifted by applying $V < |\lambda|$ which is also confirmed by Fig. 4(a). Moreover, altering V from $-\lambda$ to λ does not affect the spin Hall conductivities and corresponding Chern numbers, and C_\uparrow (C_\downarrow) always remains zero or positive (zero or negative), indicating no change in the sign of spin Hall conductivities. However, for $|V| > \lambda$, the valley Hall conductivities change their sign such that varying V from negative to positive changes the K (K') valley Hall conductivity from negative to positive (positive to negative). As the spin Hall conductivity vanishes under this condition, while the valley one is maximized, the QVH phase is confirmed, consistent with the prediction in the phase diagram in Fig. 1. In contrast, turning the laser parameters to the regime $\Delta_\Omega > \lambda$ results in a change in all phases, as shown in Fig. 4(b). When V satisfies the condition $-\Delta_\Omega + \lambda < V < \Delta_\Omega - \lambda$ [e.g., $-0.05 \text{ eV} < V < 0.05 \text{ eV}$ at $\Delta_\Omega = 1.6 \lambda$, as illustrated in Fig. 4(b)], all the Chern numbers (and therefore the Hall conductivities) become equal to 1, indicating the P-QHI phase. Note that this phase cannot be observed in the proposed structure when the off-resonance light is switched off (see Fig. 1). Outside the aforementioned interval, the Chern numbers of one specific valley and a certain spin vanish, while those of the opposite valley and spin maximize, indicating the S-QHI phase. Interestingly, applying a positive V results in a vanishing of $\sigma_{K'}$ and σ_\downarrow , while a negative electric field destroys σ_K and σ_\downarrow . This is due to the role of V in the Hamiltonian of jacutingaites, which can change the sign function and BC and consequently changes

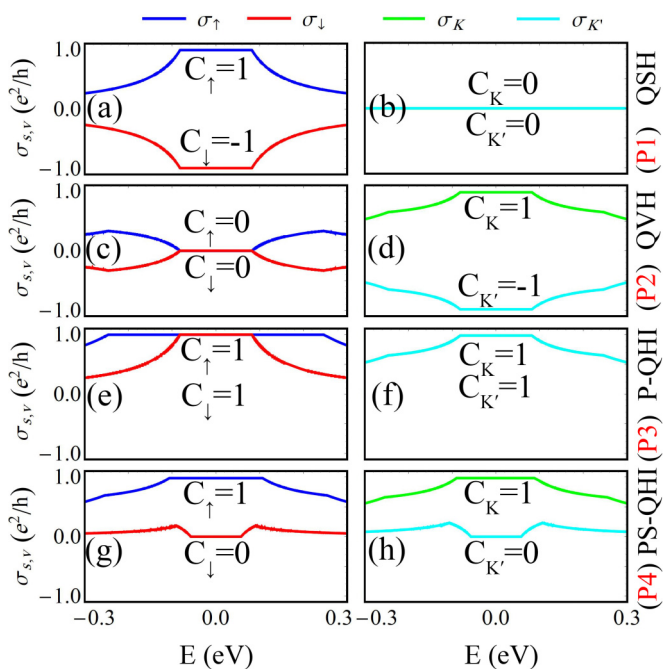


FIG. 3. Spin and valley Hall conductivities with respect to the Fermi energy at $T = 0 \text{ K}$. The first to the fourth rows refer to the P1–P4 points in the phase diagram, respectively (see Fig. 1).

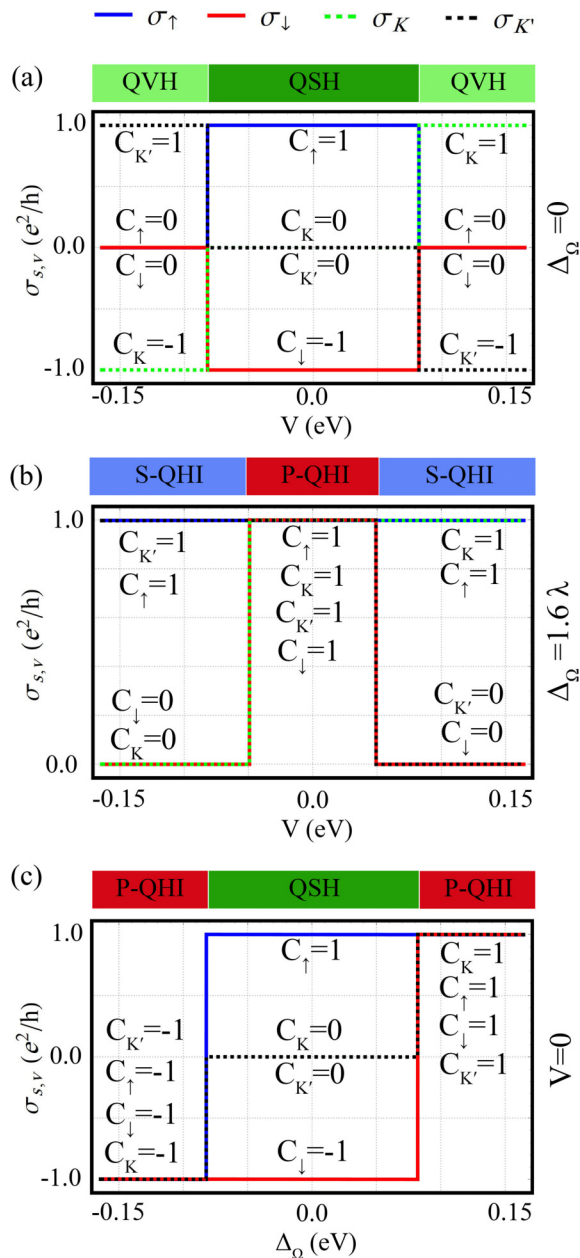


FIG. 4. The spin and valley Hall conductivities for different parameter regimes labeled in each panel with respect to (a), (b) the electric field and (c) the laser parameter. Other parameters are the same as Fig. 3.

the vanished states. In contrast to V , by considering $|\Delta_\Omega| > \lambda$ individually, reversing the light helicity from right-handed to left-handed circular polarization (referring to positive and negative Δ_Ω , respectively) can reverse all the spin and valley Hall conductivities from positive to negative. As all of the Hall conductivities are maximized at this position, the emergence of the P-QHI phase is confirmed again, as shown in Fig. 4(c). This figure indicates that the direction of the edge currents can be effectively controlled by the sign of the fields.

So far, we have investigated at zero temperature the scenario where carriers flow along the system from a source to a drain under the action of a bias voltage. However, a

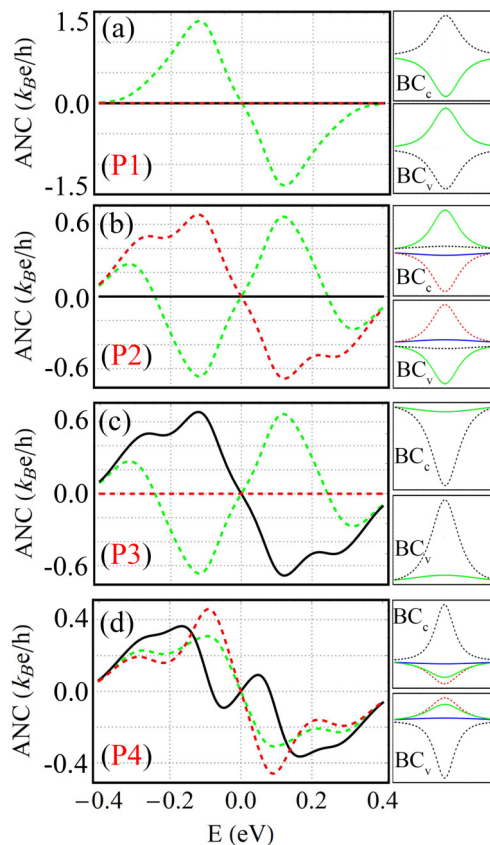


FIG. 5. The spin (SANC), valley (VANC), and total anomalous Nernst coefficient (TANC) vs the Fermi energy at $T = 300$ K for different parameter regimes corresponding to the point P1-P4 in Fig. 1. The green, red, and black curves denote the SANC, VANC, and TANC, respectively. The right panels show the corresponding BC_s for the conduction (BC_c) and valence bands (BC_v).

temperature gradient can also induce carrier flow, known as the Seebeck effect. To inspect distinct phases at elevated temperatures (which may not be measurable by Hall conductivity), the anomalous Nernst effect can be utilized, as proposed in Ref. [43]. To achieve this, a temperature gradient must be applied. We calculated for this case the transport quantities and show the SANC, VANC, and TANC as functions of Fermi energy at room temperature in Fig. 5. Since the sign of BC for conduction (BC_c) and valence (BC_v) bands is inverted, the ANC shows an odd behavior [e.g., $SANC(E_f) = -SANC(-E_f)$]. At the P1 point, where both the electric and the laser fields are turned off, the BC graphs show an overlap for different valleys at a certain spin, i.e., $\Omega_{K\uparrow} = \Omega_{K'\uparrow} = -\Omega_{K\downarrow} = -\Omega_{K'\downarrow}$, resulting in zero TANC and VANC and only nonzero SANC. This again confirms the QSH phase at the point P1 even at high temperatures. Turning on the electric field with the intensity corresponding to the point P2 breaks the degeneracies of the BC curves, leading to finite SANC and VANC. However, due to the symmetry between different spin-valley flavors, the total BC is still zero, resulting in zero TANC, as shown in Fig. 5(b). It is worth noting that this graph differs significantly from that of silicene [43], owing to the stronger SOC in jacutingaites. This significant SOC causes much more splitting in the entropy density

function's peaks, resulting in a twofold peak-dip profile observed in the ANC graph of this material. As discussed in Figs. 3 and 4 and can be seen in Fig. 5(c), the laser field (under our assumptions above) cannot affect the valleys individually, leading to degeneracy in the BC curves for the two valleys. Consequently, the VANC vanishes while TANC and SANC are finite, indicating the P-QHI phase at point P3. Applying V and Δ_Ω such that $|\pm V \pm \Delta_\Omega| > \lambda$ breaks all the degeneracies in the BC curves, resulting in nonzero values for all ANCs, indicating the S-QHI phase predicted in point P4 of Fig. 1. Thus, the Nernst diagram can effectively distinguish different phases and verify our previous predictions, offering an easier experimental approach for phase detection.

It should be noted that the phase transition in a monolayer of jacutingaite under the influence of an exchange field has been investigated in Ref. [13]. However, the ease of tuning the laser field, compared to the proximity-induced exchange fields, may prove advantageous in practical applications. Additionally, there are crucial differences between the exchange field and off-resonance laser perturbation. The most significant distinction lies in their roles within the Hamiltonian: the exchange field directly couples to the spin degree of freedom and can partially affect the gap function, whereas the laser field primarily impacts the valley state and also influences the effective gap. Consequently, the proposed system presents alternative opportunities in this field beyond previous research endeavors.

It is worth noting that when applying an electric field (unlike an off-resonance laser), it can result in ionic displacement, causing a reduction in the space group of jacutingaite from $P\bar{3}m1(164)$ to $P3m1(156)$ [14]. However, given the relative proximity of these two space groups, and considering the weak perturbations and weak laser-induced heating through pulse irradiation technique, the present model can be approximated while still maintaining the system's equilibrium. This approximation allows us to validate the main results, as demonstrated in previous studies [13,19,32]. In fact, although the ionic distortion slightly reduces the critical fields required for phase transitions, it does not disrupt the phase transitions through this type of perturbation. Considering that the displacement factor obtained in first-principle studies is approximately 0.16 \AA for a field of 1 V/\AA [14], care must be taken regarding the critical electric field, as practically it may be lower than the calculated value of 81.2 meV . However, the critical value obtained in first-principle studies ($D_z = 0.36 \text{ V/\AA}$) [14,16] is not too far from the predicted value in this paper.

IV. EXPERIMENTAL ASPECTS

Jacutingaite can be artificially synthesized through high-temperature solid-state reactions, and its mono/multilayer can be mechanically exfoliated from its bulk [1]. When a perpendicular external electric field (E_z) is present, the induced inequality of sublattice potential V leads to a sublattice staggered potential of lE_z with l being approximately 3.9 \AA [13], which is the distance between two Hg sublattices [1].

Previous theoretical studies on TMDs have employed off-resonance laser fields with energy ranging from 0.2 [24,26] to 3.3 eV [27], which is higher than the one used in this

paper, specifically, limiting light to 0.1 eV under the off-resonance (high-frequency and high-intensity) regime. This difference arises from the smaller effective gap function of jacutingaite, compared to TMDs, which results in a lower-energy threshold for the phase transition, allowing for the utilization of lower-energy scales while still operating within the off-resonance limitations. By restricting the energy range, scattering and heating effects are minimized, leading to more robust photoinduced phases, and may facilitate easier practical implementation.

Since the Fermi velocity is defined as $\hbar v_f = (\sqrt{3}/2)at$ in which $a = 7.6 \text{ \AA}$ is the lattice constant and t is the nearest neighbor hopping parameter, the minimum frequency determined by the bandwidth is on the order of 10^{14} Hz . Thus, a short laser pulse with intensity of $0.3\text{--}130 \times 10^{10} \text{ W/cm}^2$ for an eA range of $0.01\text{--}0.2 \text{ \AA}^{-1}$ can contribute with this energy [46]. This intensity is comparable to or weaker than that used in previous theoretical studies on different 2D systems [26,34]. To reduce heating effects laser short pulses should be applied, however the pulse duration should be at least a few optical cycles for the Floquet method to remain reliable. Experimental studies have demonstrated considerable valley polarization using off-resonance light with energies up to 2.33 eV , indicating the feasibility of the Floquet regime [22,23].

The Hamiltonian model employed in this paper, consistent with previous well-received research on 2D systems, offers a reasonably accurate representation of the impacts of electric and laser fields [4,18,19,34,47,48]. The findings derived from this model align with available experimental observations regarding the influence of off-resonance light on the band gap of 2D systems [22,23,49] or the properties of jacutingaite's edge states [1]. Furthermore, our results are in line with first-principle investigations that have explored the impact of electric field modulation on 2D materials [50–53], indicating the model's strong predictive capability. Although an exact experimental analogy of the proposed system may not be found in the literature, the aforementioned works show that our predictions can be experimentally feasible and can motivate future experimental studies in this field.

In general, the Rashba SOC plays a significant role in systems with broken inversion symmetry, such as electric field modulated jacutingaite [13] or proximity-induced magnetic substrate [12]. However, in the present case, the jacutingaite layer is assumed to be suspended without any magnetic or nonmagnetic substrate and consequently the effect of the Rashba SOC may not be significant. In the presence of a magnetic substrate, the Rashba SOC in jacutingaites has been estimated to be approximately 17 meV [12]. This value is considerably weaker than other energy scales employed in this paper including the laser and electric fields, and thus, it may be negligible. Notably, a recent investigation suggests that the main phases predicted in this paper can still be achieved even in the presence of Rashba SOC in a magnetized jacutingaite [13].

For practical observation of the spin Nernst effect, Yu *et al.* have proposed an H-shape detector in which the spin current, generated in the right leg by a temperature gradient, is injected into the left leg through a horizontal bridge, which can be converted into a detectable charge voltage drop by the inverse spin Hall effect [42,43].

V. SUMMARY AND CONCLUSION

In summary, we studied the various phases of a monolayer jacutingaite in a circularly polarized laser field and under the action of a staggered sublattice potential (V). In the high-frequency, high-intensity regime and after averaging over the fast time scales, the steady-state system can be described by an effective Hamiltonian which we analyzed by calculating the Chern numbers that indicate the occurrence of QSH, QVH, P-QHI, and S-QHI phases, as we vary the parameters of the laser and/or V . We also found specific states, including single Dirac cone, spin-valley-polarized metal, and spin-polarized metal, at the phase boundaries. For particular values of V and laser parameters with respect to λ , the jacutingaite monolayer exhibited a QSH state. An increase in either of the external parameters leads to the emergence of a QVH and P-QHI phase. When both fields were switched on and had a certain strength,

the system transitioned to an S-QHI phase, with $C_{\uparrow(K)} = 1$ and $C_{\downarrow(K')} = 0$. Furthermore, we demonstrated that these distinct phases can be characterized and distinguished based on the spin- and valley-Hall conductivities at low temperature and also through the Nernst coefficient calculation at room temperature.

ACKNOWLEDGMENTS

Y.H. thanks Martin-Luther Universität Halle-Wittenberg for the hospitality and support during his visit when this work was done. Y.H. also acknowledges financial support from Iran Science Elites Federation. This work has been supported by the Deutsche Forschungsgemeinschaft under Projects No. 429194455 and No. 328545488 within the SFB TRR227 project.

-
- [1] K. Kandrai, P. Vancsó, G. Kukucska, J. Koltai, G. Baranka, Á. Hoffmann, Á. Pekker, K. Kamarás, Z. E. Horváth, A. Vymazalová *et al.*, Signature of large-gap quantum spin Hall state in the layered mineral jacutingaite, *Nano Lett.* **20**, 5207 (2020).
- [2] C. L. Kane and E. J. Mele, Quantum spin Hall effect in graphene, *Phys. Rev. Lett.* **95**, 226801 (2005).
- [3] N. Mounet, M. Gibertini, P. Schwaller, D. Campi, A. Merkys, A. Marrazzo, T. Sohier, I. E. Castelli, A. Cepellotti, G. Pizzi *et al.*, Two-dimensional materials from high-throughput computational exfoliation of experimentally known compounds, *Nat. Nanotechnol.* **13**, 246 (2018).
- [4] M. Ezawa, Photoinduced topological phase transition and a single Dirac-cone state in silicene, *Phys. Rev. Lett.* **110**, 026603 (2013).
- [5] C. L. Kane and E. J. Mele, Z_2 topological order and the quantum spin Hall effect, *Phys. Rev. Lett.* **95**, 146802 (2005).
- [6] M. Ezawa, Valley-polarized metals and quantum anomalous Hall effect in silicene, *Phys. Rev. Lett.* **109**, 055502 (2012).
- [7] Z. Ni, Q. Liu, K. Tang, J. Zheng, J. Zhou, R. Qin, Z. Gao, D. Yu, and J. Lu, Tunable bandgap in silicene and germanene, *Nano Lett.* **12**, 113 (2012).
- [8] X. Qian, J. Liu, L. Fu, and J. Li, Quantum spin Hall effect in two-dimensional transition metal dichalcogenides, *Science* **346**, 1344 (2014).
- [9] L. Peng, Y. Yuan, G. Li, X. Yang, J.-J. Xian, C.-J. Yi, Y.-G. Shi, and Y.-S. Fu, Observation of topological states residing at step edges of WTe₂, *Nat. Commun.* **8**, 659 (2017).
- [10] A. Vymazalová, F. Laufek, M. Drábek, A. R. Cabral, J. Haloda, T. Sidorinová, B. Lehmann, H. F. Galbiatti, and J. Drahokoupil, Jacutingaite, Pt₂HgSe₃, a new platinum-group mineral species from the Cauê iron-ore deposit, Itabira district, Minas Gerais, Brazil, *Can. Mineral.* **50**, 431 (2012).
- [11] F. C. de Lima, R. H. Miwa, and A. Fazzio, Jacutingaite-family: A class of topological materials, *Phys. Rev. B* **102**, 235153 (2020).
- [12] Z. Liu, Y. Han, Y. Ren, Q. Niu, and Z. Qiao, Van der Waals heterostructure Pt₂HgSe₃/CrI₃ for topological valleytronics, *Phys. Rev. B* **104**, L121403 (2021).
- [13] V. Vargiamidis, P. Vasilopoulos, and N. Neophytou, Tunable topological phases in monolayer Pt₂HgSe₃ with exchange fields, *Phys. Rev. B* **106**, 205416 (2022).
- [14] A. Marrazzo, M. Gibertini, D. Campi, N. Mounet, and N. Marzari, Prediction of a large-gap and switchable Kane-Mele quantum spin Hall insulator, *Phys. Rev. Lett.* **120**, 117701 (2018).
- [15] A. Bafekry, M. Obeid, C. V. Nguyen, M. Ghergherehchi, and M. B. Tagani, Graphene hetero-multilayer on layered platinum mineral jacutingaite (Pt₂HgSe₃): Van der Waals heterostructures with novel optoelectronic and thermoelectric performances, *J. Mater. Chem. A* **8**, 13248 (2020).
- [16] L. Rademaker and M. Gibertini, Gate-tunable imbalanced Kane-Mele model in encapsulated bilayer jacutingaite, *Phys. Rev. Mater.* **5**, 044201 (2021).
- [17] Y. Hajati and Z. Rashidian, Valley and spin resonant tunneling current in ferromagnetic/nonmagnetic/ferromagnetic silicene junction, *AIP Adv.* **6**, 025307 (2016).
- [18] T. Yokoyama, Controllable valley and spin transport in ferromagnetic silicene junctions, *Phys. Rev. B* **87**, 241409(R) (2013).
- [19] D. Wang, Z. Huang, Y. Zhang, and G. Jin, Spin-valley filter and tunnel magnetoresistance in asymmetrical silicene magnetic tunnel junctions, *Phys. Rev. B* **93**, 195425 (2016).
- [20] Z. P. Niu, Spin-valley filter effect and Seebeck effect in a silicene based antiferromagnetic/ferromagnetic junction, *New J. Phys.* **21**, 093044 (2019).
- [21] K. F. Mak, K. He, J. Shan, and T. F. Heinz, Control of valley polarization in monolayer MoS₂ by optical helicity, *Nat. Nanotechnol.* **7**, 494 (2012).
- [22] S. Feng, C. Cong, S. Konabe, J. Zhang, J. Shang, Y. Chen, C. Zou, B. Cao, L. Wu, N. Peimyoo *et al.*, Engineering valley polarization of monolayer WS₂: A physical doping approach, *Small* **15**, 1805503 (2019).
- [23] B. Zhu, H. Zeng, J. Dai, Z. Gong, and X. Cui, Anomalous robust valley polarization and valley coherence in bilayer WS₂, *Proc. Natl. Acad. Sci. USA* **111**, 11606 (2014).
- [24] X.-J. Hao, R.-Y. Yuan, T. Ji, and Y. Guo, Switch effect for spin-valley electrons in monolayer WSe₂ structures subjected

- to optical field and Fermi velocity barrier, *J. Appl. Phys.* **128**, 154303 (2020).
- [25] Q. Yang, R. Yuan, and Y. Guo, Valley switch effect based on monolayer WSe₂ modulated by circularly polarized light and valley Zeeman field, *J. Phys. D* **52**, 335301 (2019).
- [26] X. Qiu, Q. Lv, and Z. Cao, Optical, electric and magnetic controlled ballistic conductance in monolayer WSe₂: The perfect valley and spin polarizations, *J. Phys. D* **50**, 455106 (2017).
- [27] X.-J. Qiu, Z.-Z. Cao, J. Hou, and C.-Y. Yang, Controlled giant magnetoresistance and spin-valley transport in an asymmetrical MoS₂ tunnel junction, *Appl. Phys. Lett.* **117**, 102401 (2020).
- [28] D.-N. Liu and Y. Guo, Optoelectronic superlattices based on 2D transition metal dichalcogenides, *Appl. Phys. Lett.* **118**, 123101 (2021).
- [29] Y. Hajati, M. Alipourzadeh, and I. Makhfudz, Spin-and valley-polarized transport and magnetoresistance in asymmetric ferromagnetic WSe₂ tunnel junctions, *Phys. Rev. B* **103**, 245435 (2021).
- [30] M. Alipourzadeh, Y. Hajati, and I. Makhfudz, Photo- and exchange-field controlled line-type resonant peaks and enhanced spin and valley polarizations in a magnetic WSe₂ junction, *J. Phys. D* **55**, 165301 (2022).
- [31] S. S. Dabiri, H. Cheraghchi, and A. Sadeghi, Light-induced topological phases in thin films of magnetically doped topological insulators, *Phys. Rev. B* **103**, 205130 (2021).
- [32] M. U. Rehman, M. Kiani, and J. Wang, Jacutingaite family: An efficient platform for coexistence of spin valley Hall effects, valley spin-valve realization, and layer spin crossover, *Phys. Rev. B* **105**, 195439 (2022).
- [33] B. Dóra, J. Cayssol, F. Simon, and R. Moessner, Optically engineering the topological properties of a spin Hall insulator, *Phys. Rev. Lett.* **108**, 056602 (2012).
- [34] T. Kitagawa, T. Oka, A. Brataas, L. Fu, and E. Demler, Transport properties of nonequilibrium systems under the application of light: Photoinduced quantum Hall insulators without Landau levels, *Phys. Rev. B* **84**, 235108 (2011).
- [35] M. Ezawa, Monolayer topological insulators: Silicene, germanene, and stanene, *J. Phys. Soc. Jpn.* **84**, 121003 (2015).
- [36] M. Katsnelson, K. Novoselov, and A. Geim, Chiral tunnelling and the Klein paradox in graphene, *Nat. phys.* **2**, 620 (2006).
- [37] M. Ezawa, Spin valleytronics in silicene: Quantum spin Hall-quantum anomalous Hall insulators and single-valley semimetals, *Phys. Rev. B* **87**, 155415 (2013).
- [38] A. Bafekry, C. Stampfl, C. Nguyen, M. Ghergherehchi, and B. Mortazavi, Tunable electronic properties of the dynamically stable layered mineral Pt₂HgSe₃ (jacutingaite), *Phys. Chem. Chem. Phys.* **22**, 24471 (2020).
- [39] D. Xiao, M.-C. Chang, and Q. Niu, Berry phase effects on electronic properties, *Rev. Mod. Phys.* **82**, 1959 (2010).
- [40] Y. Hajati, M. Alipourzadeh, and J. Berakdar, Magnetoelectric tuning of spin, valley, and layer-resolved anomalous Nernst effect in transition-metal dichalcogenides bilayers, *J. Phys.: Condens. Matter* **35**, 285602 (2023).
- [41] Y. Ren, Z. Qiao, and Q. Niu, Topological phases in two-dimensional materials: A review, *Rep. Prog. Phys.* **79**, 066501 (2016).
- [42] X.-Q. Yu, Z.-G. Zhu, G. Su, and A.-P. Jauho, Thermally driven pure spin and valley currents via the anomalous Nernst effect in monolayer group-VI dichalcogenides, *Phys. Rev. Lett.* **115**, 246601 (2015).
- [43] Y. Xu, X. Zhou, and G. Jin, Detecting topological phases in silicene by anomalous Nernst effect, *Appl. Phys. Lett.* **108**, 203104 (2016).
- [44] N. Missault, P. Vasilopoulos, V. Vargiamidis, F. M. Peeters, and B. Van Duppen, Spin-and valley-dependent transport through arrays of ferromagnetic silicene junctions, *Phys. Rev. B* **92**, 195423 (2015).
- [45] Z. P. Niu and S. Dong, Controllable valley and spin-polarized transport and negative magnetoresistance in a silicene junction, *Europhys. Lett.* **111**, 67003 (2015).
- [46] S. Li, C.-C. Liu, and Y. Yao, Floquet high Chern insulators in periodically driven chirally stacked multilayer graphene, *New J. Phys.* **20**, 033025 (2018).
- [47] Z. Gong, G.-B. Liu, H. Yu, D. Xiao, X. Cui, X. Xu, and W. Yao, Magnetoelectric effects and valley-controlled spin quantum gates in transition metal dichalcogenide bilayers, *Nat. Commun.* **4**, 2053 (2013).
- [48] H. Khani and S. P. Pishekloo, Gate-controlled spin-valley-layer locking in bilayer transition-metal dichalcogenides, *Nanoscale* **12**, 22281 (2020).
- [49] L. Huang, Y. Wang, H. Su, G. Hu, C. Deng, Y. Sun, B. Yun, R. Zhang, Y. Chen, F. Wang *et al.*, Manipulating valley-polarized photoluminescence of MoS₂ monolayer at off resonance wavelength with a double-resonance strategy, *Appl. Phys. Lett.* **119**, 031106 (2021).
- [50] N. D. Drummond, V. Zolyomi, and V. I. Fal'Ko, Electrically tunable band gap in silicene, *Phys. Rev. B* **85**, 075423 (2012).
- [51] E. Zaminpayma and P. Nayebi, Band gap engineering in silicene: A theoretical study of density functional tight-binding theory, *Physica E* **84**, 555 (2016).
- [52] J.-A. Yan, S.-P. Gao, R. Stein, and G. Coard, Tuning the electronic structure of silicene and germanene by biaxial strain and electric field, *Phys. Rev. B* **91**, 245403 (2015).
- [53] C. Lian and J. Ni, The effects of thermal and electric fields on the electronic structures of silicene, *Phys. Chem. Chem. Phys.* **17**, 13366 (2015).